12WCEE 2000

EMERGENCE OF WATER FILM IN LIQUEFIED SAND AND ITS ROLE IN LATERAL FLOW

Takeji KOKUSHO[1], Tetsuro KOJIMA[2] And Nozomi NONAKA[3]

SUMMARY

1G shake table tests are carried out for two-dimensional slope models with seams of silt within a saturated sand. Water films formed beneath silt seams enables soil mass above them to laterally flow along water films not only during but also after shaking, while the soil deforms mostly during shaking and almost stops after that in the case without silt. The dilatancy effect exerted in sheared sand during flow failure is discussed in relation with the water film generation based on the measurement on shear strain. In view of the significant role of the water film, a mechanism for the emergence of a water film in a layered sand is studied in a simple one-dimensional model test. It is clarified that upward seepage force exerted in a sandwiched layer with a smaller permeability and an overlying reaction layer are essential to a stable formation of a water film.

INTRODUCTION

A close look at a natural sand layer readily reveals that it normally consists of a set of sub-layers with different soil particles including silty sands and coarse sands due to stratification process. In Niigata, for example, where extensive lateral flow occurred during the 1964 Niigata earthquake (Kawakami and Asada, 1966), subsoil conditions based on boring logs indicates that the soil consists of various sub-layers as shown in Fig.1 (Kishida 1966). In artificially reclaimed soils, stratification sometimes tends to become more pronounced. If such a sand layer liquefies, it is highly probable that excess pore-water squeezed from the liquefied sand is trapped by relatively impermeable sub-layers and forms water films beneath them. Despite a probable involvement of water films and its potential role in a lateral flow failure, a smaller number of researches have focused on water films in the mechanism of the lateral flow failure.

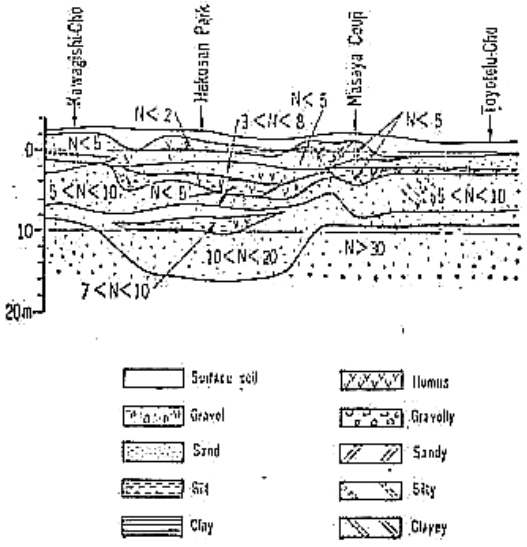

Fig.1 Soil profile along a line through Hakusan District in Niigata City (Kishida 1966)

The present author and his group (Kokusho and Watanabe 1997, Kokusho et al. 1998 and Kokusho 1999) have systematically investigated a generation of water film beneath a thin silt seam and its significant role in lateral flow mechanism by small-scale model tests. In the first part of this paper, 1-G shake table test results will be discussed to demonstrate the water film effect involved in the mechanism of lateral flow. In the latter

[1] *Faculty of Science and Engineering, Chuo University, 1-13-27 Kasuga, Bunkyo-ku, Tokyo,112-8551 JAPAN*
[2] *Faculty of Science and Engineering, Chuo University, 1-13-27 Kasuga, Bunkyo-ku, Tokyo,112-8551 JAPAN*
[3] *Faculty of Science and Engineering, Chuo University, 1-13-27 Kasuga, Bunkyo-ku, Tokyo,112-8551 JAPAN*

part, in view of the significant role of water film in a liquefied sand layer, the mechanism of water film generation will be closely studied through a series of one-dimensional model tests.

MODEL TEST ON LATERAL FLOW IN SLOPING GROUND WITH AN ARC OF SILT

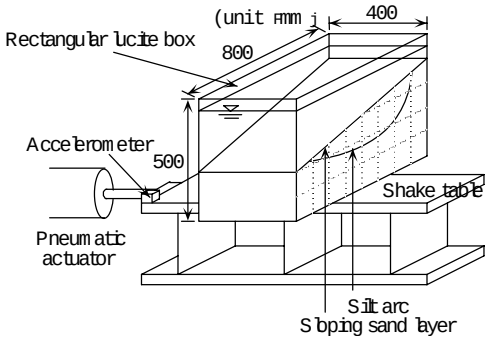

Fig.2 Two-dimensional model for saturated sand slope with a silt arc in a lucite box on a shake table

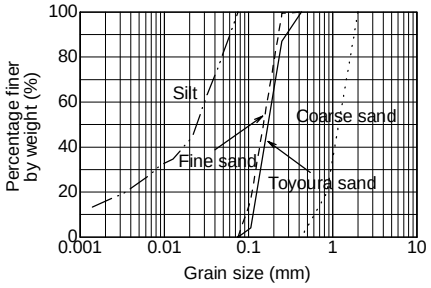

Fig.3 Grain size curves for soil materials used in this research

A rectangular lucite soil box with a section of 500mm in height, 800mm in width and 400mm in thickness is filled with water, and fine sand is rained to make a saturated loose sand layer. An arc of silt is introduced in it as shown in Fig.2 to represent a less pervious sublayer in the field. The thickness of the silt seam is 6 mm in average, although it varies from 2 to 8 mm from part to part. The grain size curve for the fine sand and the silt is available in Fig.3. A comparative test with the same configuration but without the silt arc is also carried out. The model is liquefied with a kind of repetitive motions of 3 Hz with the acceleration of about 0.3 G. The direction of shaking is perpendicular to the sloping direction as shown in Fig.2 so that the effect of the inertia force be excluded in the lateral flow deformation. Failure modes in these tests are visualized by movements of marker grids made from Japanese noodles attached to the transparent wall of the box.

In Figs.4 (a) and (b), the movements of the slope with a silt arc, case 1 and case 2, during and after shaking are illustrated in two separate charts, respectively. In Fig.4 (c) the same chart without silt is illustrated. The relative density, Dr, for case 1,2 and 3 is 36%, 21% and 19%, respectively. The maximum and minimum density of the sand is evaluated by the standard test method by the Japanese Geotechnical Society. If no silt arc exists, the slope deforms continuously without any discontinuous slip surface, and major movement stops as soon as the shaking stops. It should be noted here that the 100% pore-pressure build-up is still maintained at the end of shaking (Kokusho and Watanabe 1997). With silt, a discontinuity in flow deformation at the silt arc becomes dominant and the slope deforms not only during shaking but also after shaking. Without silt, the deformed area extends into a deeper part of the cross-section leading to a larger area of shear deformation. In contrast to that, only a

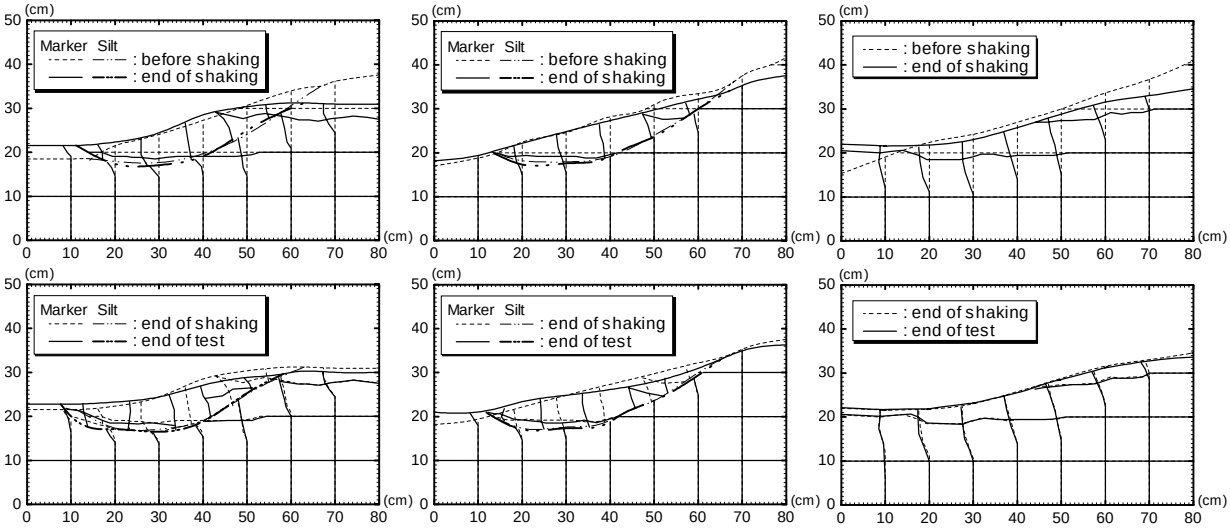

(a) case1 with a silt arc (b) case 2 with a silt arc (c) case 3 without a silt arc

Fig.4 Deformation of sloping sand during shaking (top) and after shaking (bottom)

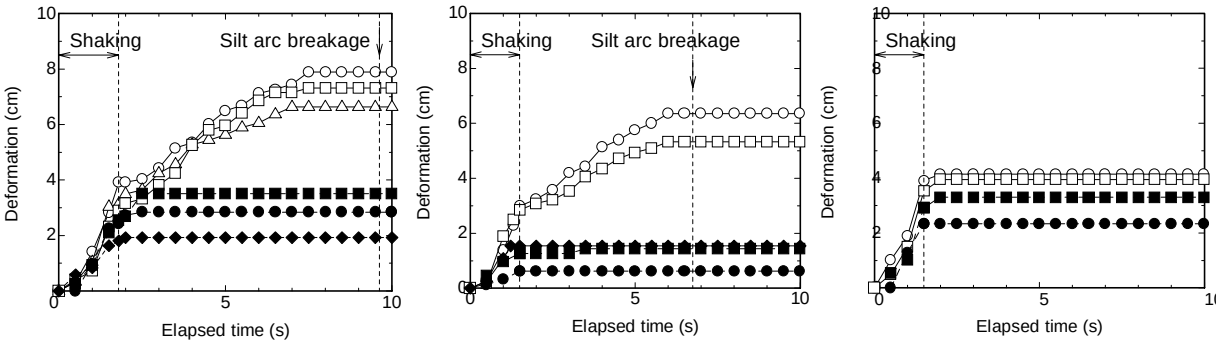

(a) case1 with a silt arc (b) case 2 with a silt arc (c)case 3 without a silt arc

Fig.5 Soil deformation versus elapsed time relationship for representative points in sloping sand

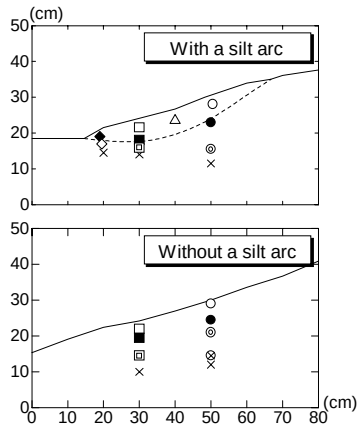

Fig.6 Location of representative points in the cross-section of slope corresponding to different symbols in Fig.5 and Fig.7

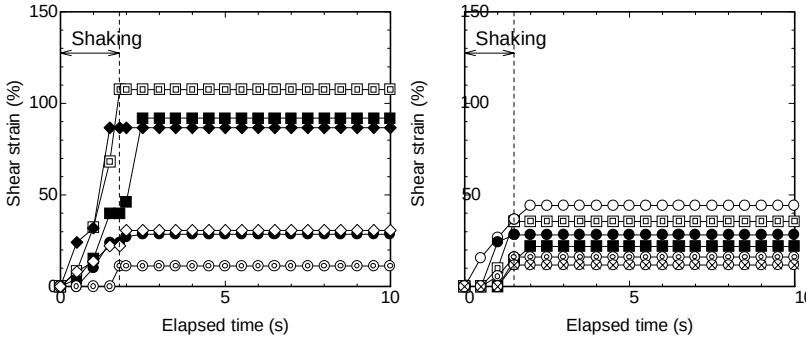

(a) case 1 with a silt arc (b) case 2 without a silt arc

Fig.7 Shear strain versus elapsed time relationship for representative points in sloping sand

narrow or almost no area of shear deformation develops just below the silt arc in the case with silt.

Figs5. (a) and (b) show time-dependent variations in deformation (a scalar sum of the length of deformation increment vector for each time increment) at representative points in the slope with the silt arc, while Fig5.(c) shows those in the slope without silt. The symbols in Figs5.(a) to (c) correspond to locations in the cross-section shown in Fig.6. In these charts the time interval of shaking and the moment when the silt seam is broken due to upward seepage flow is indicated. It is obvious from this figure that the soil mass above the silt arc symbolled with open marks continues to deform still after the end of shaking while the points just below the arc symbolled with close marks stop as soon as the shaking stops. In contrast, the slope without silt deforms mostly during shaking. Visual observation reveals that as soon as the shaking starts a thin water film shows up at the lower part in the silt seam, which continues to exist until the breakage of the silt, while some of it rushes out to the surface through the ends of arc. The slide obviously takes place along the water film during the period when it is sustained beneath the arc.

Such a basic question may arise on the initial emergence and sustainability of a water film during flow-failure; As shown in Fig.4, the sand deforms mostly in a shear mode, which will cause the dilatancy effect. If a water film emerges, the sand underneath is under ultra-low confining stress, which may farther dilate the sand, absorbing ambient water and prohibiting the generation of water film as well as the flow-failure along it.

In order to find a key to this question, shear strain is read off from Figs.4(a) and (c) for cases with and without silt arcs and plotted versus time in Figs.7(a) and (b), respectively. The shear strain γ is calculated in the two cases along vertical markers shown in Figs.6(a) and (b) for the intervals above the cross mark. Shear strain of 10 to 40 % is induced in the sand during shaking in the case without silt.

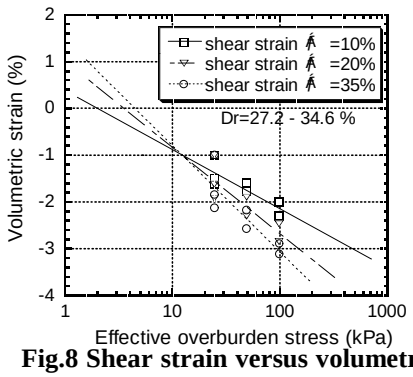

Fig.8 Shear strain versus volumetric strain relationship of loose sand measured with simple shear apparatus for three vertical stresses (Kokusho and Nakano 1999)

In Fig.8, a volumetric strain measured by a drained simple shear test is shown for the same sand of Dr≈30% under different vertical stresses, σ_v' , which are actually much higher than those for the model test (Kokusho and Nakano 1999). The dilatant behavior of the sand is quite dependent on the vertical effective stress. Even for the lowest stress of σ_v' = 25 kPa, the sand contracts down to 2% volumetric strain up to the shear strain of 35%. However, it may be estimated by a linear extrapolation on the semi-log chart that the sand in the model exhibits a dilation of about 1% volumetric strain under a ultra-low confining stress of as low as 1 kPa for the shear strain of 35%. In a drained condition, the volumetric strain seems to be large enough to absorb at least a part of the excess pore-water coming out from a liquefied sand layer if the post liquefaction settlement is of the same order. In an undrained condition, this dilatant behavior will increase the effective stress in the sand and the slope will stop its flow movement as soon as the excess pore-pressure during shaking disappears.

In the case with a silt arc the shear-deformed area develops very little as shown in Fig.4(b) or develops to a smaller extent as in Fig.4(a) than the case without silt although the local strain grows up to about 100% near the down-slope side. This restriction in development of the shear-deformed area under the silt may be attributable to the water film, which, once emerging, will transmit no shear stress to the lower sand.

The results of these model tests are of course quite qualitative and therefore large scale model tests or centrifuge tests will be needed to draw more quantitative results. However the following considerations based on the model test results will provide a valuable insight in the flow failure mechanism in the field. The effective confining stress at the slip surface in this test is about 0.5 to 2 kPa and very much lower than the field stress. As shown in Fig.8, sand tends to be much more contractive under higher confining stress and thus undoubtedly leads to more dominant water film effect in the field. Because it has been demonstrated in the model that a water film is easily formed beneath a silt seam in a very dilative environment and serve as a sliding surface for lateral flow failure, the same mechanism will surely be involved in lateral flow failure in the field.

MECNANISM FOR WATER FILM FORMATION

In view of the significance of the water film involvement in flow failure mechanism, a series of model tests for a one-dimensional layer sand are carried out to systematically study the mechanism for water film generation. Three types of layered soil models are tested in a one-dimensional test tube.

In the first model a saturated loose sand layer is made by pouring dry Toyoura sand into water in a lucite tube of 13.0cm in inner diameter and 211.5cm in height as illustrated in Fig.9. The sand layer of 200cm in depth sandwiches a seam of non-plastic silt in the middle (96cm from the bottom) to separate the upper and lower sand layers. The grain size distributions of the tested soils are available in Fig.3. The relative density, Dr, of the lower layer is adjusted to have values as listed in Table 1. 50 gram of silt is used to make a silt seam of about 4 mm thick. The permeability constants for this silt seam and the upper sand layer are 10^{-4}cm/s and 10^{-2}cm/s.

The one-dimensional sand layer is instantaneously liquefied by a shock given by a steel hammer powered by a controlled spring force. The shock causes the final settlement of about 3% maximum of the total soil thickness. This percentage is almost the same compared to what was estimated in the Niigata city during the 1964 Niigata earthquake (Ishihara 1996). Five electric pore-pressure gages are installed at five levels of the tube as shown in Fig.9 to measure excess pore-pressure during and after liquefaction. The settlement of the sand and the thickness of the water film are measured by two digital video-cameras to have their time-dependent records.
In Fig.10, a typical result for the case with a silt seam is shown; the settlements at the top of the upper and lower layers (at z=200cm and z=96cm respectively where z-axis is taken vertically from the bottom of the sand layer) are plotted against the elapsed time starting at the moment of shock. In the same figure the variation in thickness of the water film beneath the silt seam is also plotted. It is readily understood that the water film starts to show up just after the onset of complete liquefaction. This indicates that the undrained condition does not hold locally but a migration of pore-water occurs in a very short time period. In the figure, the start, the end and the turning points of the curves are benchmarked as p1 through p5. It is evident that p2 and p3 correspond to the completion

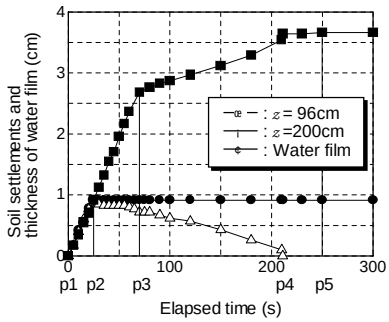

Fig.10 Time-dependent variation in water film thickness and soil settlement in sand layer with a seam of silt compared with analysis

of the sedimentation in the lower and upper sand layers, respectively. The water film beneath the silt seam grows to its maximum thickness at p2 with almost the same speed as the settlement of the lower layer. After that it decreases thickness due to a seepage flow through the silt and the upper sand layer until it vanishes at point p4. At the same time the settlement in the upper layer continues with slower rate up to point p5, which corresponds to the consolidation due to remained excess pore-pressure.

Based on the five pressure-gage readings, excess pore-pressure distributions along the depth are plotted in Fig.11. The pressure in the upper layer is evidently varied with depth, indicating clear influence of upward flow from the water film. It is also noted that, by extrapolating the pressure gradient from upper and lower layers, there exists a distinctive gap in pressure at the silt seam, introducing a high hydraulic gradient in it.

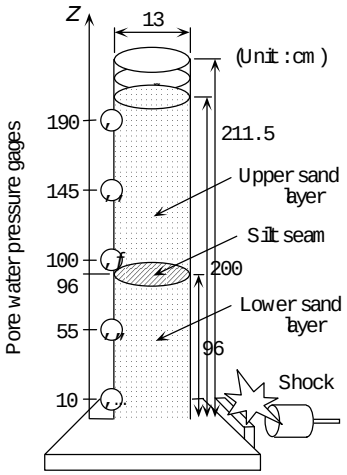

Fig.9 One-dimensional model of saturated loose sand instantaneously liquefied by a hammer

It can readily be understood that, if there is a water film formed in a soil layer continuously in horizontal direction, the excess pore-pressure in the soil layer below should equal to the initial effective overburden stress so long as the water film is sustained. However, the measurements in the lower pressure gages actually decrease down to much lower value as indicated in Fig.11. This may be attributable to the skin friction between the inside wall of the tube and the sand (Kokusho 1999). The excess pressure in the field would stay at the overburden effective stress as long as the water film exists. In the meantime the excess pressure in the upper layer decrease due to post-liquefaction pressure dissipation, leading to much higher hydraulic gradient in the silt seam than in the model.

The second model consists of two layers of 90cm in each thickness; upper fine sand and lower coarse sand, the grain size curves of which are shown in Fig.3 made in the same test tube shown in Fig.2. As soon as the sand instantaneously liquefies after the hammering, a fierce turbulance shows up at the boundary of the two layers due to the excess water comming out of the lower coarse sand. This phenomenon introduces a thin zone of larger void ratio, which greatly differs from the water film formed beneath the silt seam in quality and stability. The turbulance stays only for a few seconds at the boundary and then fades away into the upper layer. In Fig.12, settlements at the surface and the boundary are plotted versus the elapsed time. While the boundary finishes its settlement in a very short time, the surface keeps settling with much lower rate, indicating that the upper sand layer experiences a volume expansion between the time interval p2-p3 presumably due to the upward seepage flow from the lower coarse sand layer.

Fig.13 depicts the time-dependent change in pore-pressure distribution along depth for the same test. It is clearly seen that, unlike the case for the sandwiched silt seam, the pressure dissipation takes place in sequence from the bottom to the top and no distinct pressure gap seems to exist at the layer boundary. The upper sand layer still stays mostly liquefied at p3 (t=20s.). After that moment the upper layer starts to settle as shown in Fig.12.

Table 1 Soil parameters for the one-dimensional model tests

	Sandwiched silt seam model			Two-layers model			Three-layers model		
Layer	Soil material	Layer thickness (cm)	Relative density (%)	Soil material	Layer thickness (cm)	Relative density (%)	Soil material	Layer thickness (cm)	Relative density (%)
Upper	Fine sand	103	14	Fine sand	90	39	Coarse sand	93	30
Middle	Silt	0.4	-	-	-	-	Fine sand	5	48
Lower	Fine sand	96	39	Coarse sand	90	37	Coarse sand	97	44

The third model consists of three layers: upper and lower coarse sands and middle sandwiched fine sand, the thickness of which are 93cm, 97cm and 5cm, respectively. In this case a stable water film can be seen beneath the fine sand layer in the middle. A time-dependent variations in the settlements at the surface and the top of the lower layer as well as the water film thickness are shown in Fig.14. This indicates a strong similarity to the case for the sandwiched silt seam although the time duration is much shorter in this case because of the higher permeability in sands. The surface settles simultaneously with the top of the lower layer and the water film grows until the end of settlment in the lower layer, p2. After p2, the water film reduces its thickness and dissappears at p3 at almost the same pace with the surface settlement. The vertical pressure distribution in Fig.15 indicates that the pressure dissipates both at the lower and upper layers at the same time. On account of this concurrent resedimentation from liquefaction, a high hydraulic gradient is induced in the sandwiched middle layer. This gradient acts an upward seepage force on the middle layer and pushes it up against the overlying resolidified upper layer, enabling the water film to keep staying beneath it.

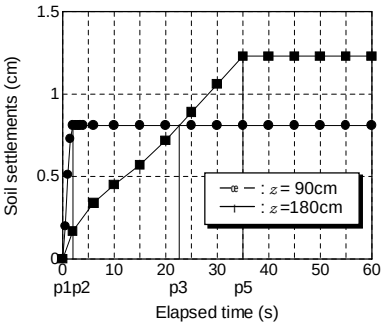

Fig.12 Time-dependent variation in soil settlement in two-layers model

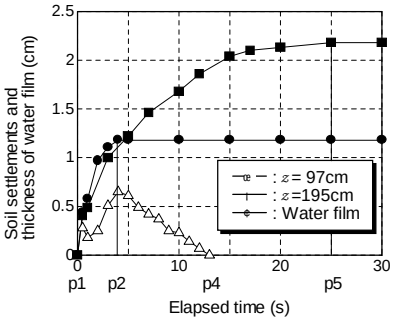

Fig.14 Time-dependent variation in soil settlement in three-layers model

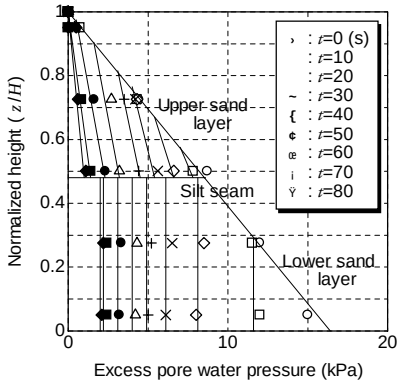

Fig.11 Time-dependent variation in excess pore-pressure distribution along depth with a silt seam

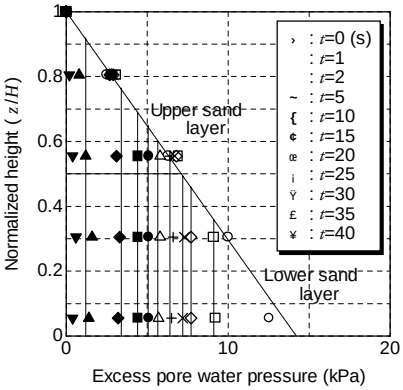

Fig.13 Time-dependent variation in excess pore-pressure distribution along depth in two-layers model

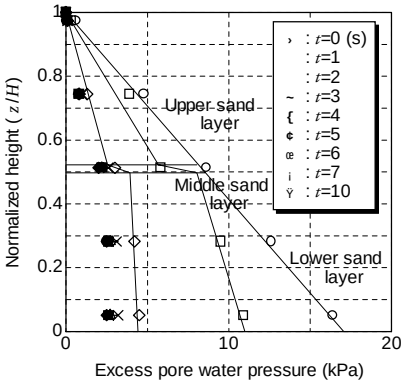

Fig.15 Time-dependent variation in excess pore-pressure distribution along depth in three-layers model

It is readily understood from the sketch in Fig.16 that, once a water film is formed beneath the middle layer, the hydraulic gradients in the layers are correlated by the equation

$$i_m H_m + i_u H_u = \alpha\left(\frac{\gamma'_m}{\gamma_w} H_m + \frac{\gamma'_u}{\gamma_w} H_u\right) \qquad (1)$$

where i_m, i_u = the hydraulic gradient in the middle or upper layer, H_m, H_u = the thickness of those layers, γ_m', γ_u'= the buoyant unit weight of those layers and γ_w = the unit weight of water. A constant α in the

$$i_m k_m = i_u k_u \qquad (2)$$

equation, which takes between unity and zero, represents the reduction rate of the effective overburden stress due to the skin friction along the inner wall of the test tube. Because of the equality of the apparent seepage velocity in the middle and upper layers,

where k_m, k_u = the permeability coefficient in those layers. By combining Eqs.(1) and (2), the gradient in the

$$i_m = \frac{\alpha\left(\gamma'_m H_m + \gamma'_u H_u\right)/\gamma_w}{H_m + \left(k_m/k_u\right)H_u} \qquad (3)$$

middle layer, i_m, is expressed as

A condition for forming a stable water film is that the seepage force by this gradient $i_m \gamma_w$ exceeds the buoyant weight of the middle layer γ_m', which results in the

$$H_m < \frac{\alpha\gamma'_u - \left(k_m/k_u\right)\gamma'_m}{\left(1-\alpha\right)\gamma'_m} H_u \qquad (4)$$

following inequality for the thickness of the middle layer.

Normally the difference in the unit buoyant weight between soils may be neglected; $\gamma_m' \approx \gamma_u'$, then the critical thickness, H_{mcr} , for forming a stable water film is

In the field, α=1.0 and H_{mcr} becomes infinity, which indicates no matter how thick the middle layer is, a stable water film will appear beneath it.

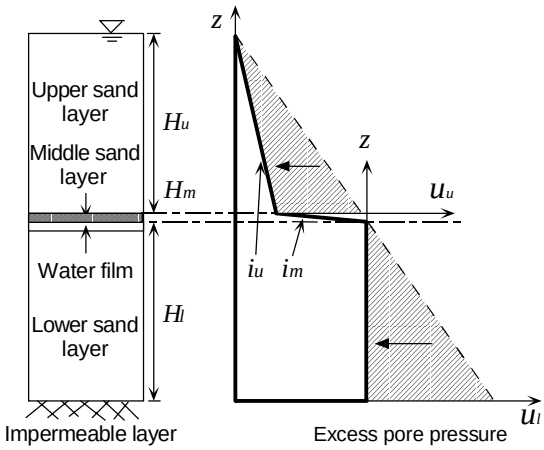

Fig.16 Conceptual diagram for water film formation

Based on these simplified considerations, a water film will emerge in the field beneath a fine-coarse boundary so long as there exists a solid layer above the upper finer soil layer which can reacts the upward seepage force.

$$H_{mcr} = \frac{\alpha - \left(k_m/k_u\right)}{\left(1-\alpha\right)} H_u \qquad (5)$$

Soils recovered from liquefaction non-liquefiable soils and also unsaturated soils which normally caps a liquefiable layer in the field may possibly serve as a reaction layer and generate a stable water film beneath a fine-coarse boundary.

CONCLUSIONS

1) If a water film is continuously formed beneath a silt seam in a sand with a lateral flow potential, it is possible for a soil mass even with a very gentle slope to be driven only by gravity force even after the end of shaking, which was sometimes observed in the field.

2) The shear deformation during lateral flow is normally expected to dilate the sand, increasing the effective stress in the undrained condition or absorbing ambient water in drained condition. The area of shear deformation is actually very much limited beneath the silt seam if a water film is formed in contrast to a uniform sand layer without water film, probably because the shear stress caused by a driving force is interrupted by a water film, failing to reach the sand below. This may help the water film exist during flow failure without being absorbed in dilatant sand.

3) A water film is easily formed beneath a silt seam in a short time period after liquefaction in a loose sand layer, indicating a local migration of pore-water cannot be neglected. A water film tends to outlive post-liquefaction resolidification in sand part and thus may affect soil stability longer than apparent time period of liquefaction.

4) A simple two layers system will not make a stable water film but only a short-life turbulance. A three layers system with a sandwiched middle layer of finer soil can generate a stable water film.

5) Essential mechanism for a stable water film generation involves an upward seepage force pushing up the middle layer against a upper reaction layer. Resolidified saturated layer as well as unsaturated surface layer may serve as the reaction layer.

Based on the above-mentioned experimental findings, it is highly probable that the water film effect has a significant role in a lateral flow failure in liquefied loose sand layer in the field. Because water films will easily be formed beneath less permeable sub-layers , they are surely chosen as a part of sliding surface for lateral spreading failure. The failure may occur not only during but also after earthquake shaking as demonstrated in this study.

REFERENCES

Ishihara,K. (1996) Soil behaviour in earthquake geotechnics, Oxford Science Publications

Kawakami,F. and Asada,A. (1966) Damage to the ground and earthstructures by the Niigata earthquake of June 16, 1964, Soils and foundations, Vol.Ⅳ, No.1, pp14-30.

Kishida,H. (1966) Damage to reinforced concrete buildings in Niigata City with special reference to foundation engineering, Soils and Foundations, Vol.VI, No.1, pp71-88.

Kokusho,T. and Watanabe,K. (1997) Water film effect on lateral flow in liquefied ground, Proc. of Earthquake

Engineering Symposium, Japan Society for Civil Engineers (in Japanese), pp545-548.

Kokusho,T. , Watanabe,K. and Sawano,T. (1998) Effect of water film on lateral flow failure of liquefied sand, Proc. 11th European Conference on Earthquake Engineering (Paris)

Kokusho,T. (1999) Formation of water film in liquefied sand and its effect on lateral spread, Journal of Geotechnical Engineering Division, ASCE, in print

Kokusho,T. and Nakano,T. (1999) Volume change characteristics of gravelly soils by means of simple shear test, Proc. Of Annual Convention of Japan Geotechnical Society, in print (in Japanese)